Publisher: GSA
Journal: GEOL: Geology
DOI:10.1130/G39287.1

Thin crust and exposed mantle control sulfide differentiation in slow-spreading ridge magmas

Jakub Ciazela[1,2*], Henry J.B. Dick[3], Juergen Koepke[1], Bartosz Pieterek[2], Andrzej Muszynski[2], Roman Botcharnikov[1,4], and Thomas Kuhn[5]

[1]*Institut für Mineralogie, Leibniz Universität Hannover, Callinstr. 3, 30167 Hanover, Germany*

[2]*Institute of Geology, Adam Mickiewicz University, ul. Bogumiła Krygowskiego 12, 61-680 Poznań, Poland*

[3]*Department of Geology and Geophysics, Woods Hole Oceanographic Institution, MS #8, McLean Laboratory, Woods Hole, Massachusetts 02543-1539, USA*

[4]*Institut für Geowissenschaften, Guttenberg Universität Mainz, J.-J. Becher Weg 21, 55128 Mainz, Germany*

[5]*Bundesanstalt für Geowissenschaften und Rohstoffe, Stilleweg 2, 30655 Hanover, Germany*

*E-mail: j.ciazela@mineralogie·uni-hannover.de; phone: +49 511 762 2322

ABSTRACT

Gabbroic veins enclosed in mantle peridotite from ocean core complexes next to oceanic transform faults demonstrate sub-crustal crystallization of silicate minerals from a MORB-like melt. Cooler lithosphere there may also affect sulfide crystallization and the metal budget of the lower and upper crust but the related sulfide behavior is poorly understood. Here, we use chalcophile elements to trace sulfide crystallization in a suite of MORBs erupted at the Kane Megamullion south of the Kane Fracture Zone along the

Publisher: GSA
Journal: GEOL: Geology
DOI:10.1130/G39287.1

Mid-Atlantic Ridge. Cool lithosphere there is inferred from a low magma supply, and lithostratigraphic evidence for thin crust with abundant mantle rock exposed to the seafloor (Dick et al., 2008). We show that the concentrations of Cu, Zn, As, Ga, Pb, Sb and Tl in the Kane Megamullion MORBs rise linearly with melt differentiation expressed by decreasing MgO and Ni content. The low-pressure fractional crystallization within the crust thus occurs at sulfide-undersaturated conditions. Sulfide-undersaturated MORBs are unusual. At the Kane Megamullion, however, the thin crust allows melt to more extensively interact with the shallow and serpentinized mantle. We argue that sulfur and chalcophile elements have been lost from the melt due to sulfide crystallization during melt-rock reaction in the shallow mantle.

INTRODUCTION

Mid-ocean ridge basalts (MORB) are both the most abundant and the most-studied rocks from the Earth's oceans, and represent 75% of the Earth's annual magma production (Crisp, 1984). The main process controlling MORBs differentiation is low-pressure fractional crystallization of olivine, plagioclase, and clinopyroxene within the crust (White and Klein, 2013). Sulfides also appear to form there as chalcophile element concentrations decrease gradually with MORB differentiation (Jenner and O'Neill, 2012; Francis, 1990). This implies that, on average, cumulates in the lower ocean crust would be richer in chalcophile elements than the overlying lavas and dikes. However, the global average gabbro Cu concentration (71 ± 19 ppm, σ; Coogan, 2014) appears lower than the global average MORB Cu concentration (81 ± 25 ppm, σ; White and Klein, 2013), and much lower than in the primitive MORBs (~120 ppm Cu; Lee et al. 2012). An appealing way to explain this discrepancy would be to assume that a significant portion of sulfide

crystallization occurs in the shallow mantle. The general concept of sub-crustal crystallization is already well known for silicate minerals (White and Klein, 2013). Early crystallization can be triggered by a thicker cooler lithosphere at slow-spreading ridges, particularly in regions with lower magma supply as in the vicinity of fracture zones (Herzberg, 2004; Villiger et al., 2007). However, little is known about: 1) the extent to which sulfides are involved in sub-crustal differentiation; 2) what the principle crystallization mechanism is; and 3) what the implications for the subsequent differentiation of chalcophile elements in the crust are.

In order to understand the effect of a cooler lithosphere on sub-crustal sulfide crystallization, we investigated a suite of MORBs from a region of thin crust indicative of low magma supply from the slow-spreading Mid-Atlantic Ridge (MAR). We find they have an anomalous pattern of chalcophile element differentiation with respect to typical MORBs. We interpret this pattern as caused by sub-crustal sulfide precipitation during melt interaction with the shallow mantle.

SAMPLES

The studied MORBs come from the Kane Megamullion ocean core complex (OCC) adjacent to the Kane Fracture Zone (23°38'N) at the MAR (Dick et al., 2008). As with other OCC's, Kane Megamullion exposes lower crust and mantle rocks in the footwall of a detachment fault. Oceanic detachment faults are long-lived low-angle plutonic growth faults that usually form along slow-spreading ridges during periods of low to intermediate magma supply (Cann et al., 1997; Tucholke et al., 1998). Basalt carapace on the seafloor is discontinuous. Dick et al. (2008) mapped the extent of the lavas and interpret it to have either erupted off axis, or to be a remnant of the hanging

wall. We have selected nine cogenetic MORBs collected during Jason II Dives 110 and 111, and Dredge 1 from one pillow basalt formation (23°34'N, 45°19'W) located ~5 km south of the Kane Fracture Zone (Dick et al. 2008). All our samples are undeformed, minimally seafloor weathered to fresh, aphyric (cryptocrystalline) to 1%-olivine-phyric basalts. Two samples preserve glassy rims. The cryptocrystalline matrix is largely plagioclase, olivine and clinopyroxene with minor titanomagnetite and ilmenite.

METHODS

Whole-rock major element contents were analyzed by X-ray Fluorescence (XRF) spectroscopy at the Federal Institute for Geosciences and Natural Resources, Hanover, Germany. An ELTRA CS 800 carbon/sulfur Analyzer (Institute of Mineralogy, Leibniz University of Hanover, Germany) was used to determine whole-rock sulfur contents using the analytical procedure of Lissner et al. (2014). Chalcophile element concentrations were determined by a combination of instrumental neutron activation analysis (INAA), and inductively coupled plasma - mass spectrometry (ICPMS), both conducted by Activation Laboratories Ltd., Ontario, Canada with the Ultratrace 5 analytical package. Mineral major and trace element compositions were determined with a Cameca SX100 electron microprobe (EPM) and an ELEMENT-XR (Thermo Scientific, Germany) fast-scanning sector field inductively coupled plasma ICPMS coupled to a femtosecond laser ablation (fs-LA) system (Solstice, Spectra-Physics, USA) at the Institute of Mineralogy, Leibniz University of Hanover, Germany.

RESULTS

Major and trace element compositions of the whole-rock samples as well as for olivine, plagioclase, and clinopyroxene are reported in the Data Repository (Tables DR1–

Publisher: GSA
Journal: GEOL: Geology
DOI:10.1130/G39287.1

4). Our glasses and whole-rock samples have MgO contents between 8.3% and 6.1% (Fig. 1) suggesting that the basalts represent moderately evolved mid-ocean ridge melts. Compositions of both investigated glasses are consistent within 5% with the respective whole-rocks (Fig. 1). A high Na_8 of 3.1% (Na_2O content normalized to 8 wt.% MgO; Klein and Langmuir, 1987) is in agreement with the high Na_8 found in other MORBs formed under the thin crust at the Southwest Indian Ridge, the Gakkel Ridge, and the MAR from 13° to 35°N (White and Klein, 2013).

The basalts display a Cu trend that contrasts with the global MORB trend: between 8.3–6.0 wt.% MgO, Cu increases linearly from 60 to 100 ppm with a coefficient of determination (R^2) of 0.90, whereas non-plume-related MORBs from the global reference data set of Jenner and O'Neill (2012) show the Cu concentrations decreasing from 80 to 60 ppm over the same MgO range (Fig. 1). The increasing Cu trend in the Kane Megamullion MORBs is matched by increasing Zn, As, Pb, Tl, Sb, and Ga. For example, Zn rises from 85 to 115 ppm with decreasing MgO (R^2 = 0.94; Fig. 2). Similar trends are observed against another differentiation index, the Ni content, with R^2 values of 0.86 for Cu, and 0.71 for Zn. Chalcophile elements thus behaved incompatibly during the differentiation of the Kane Megamullion MORBs, implying that this occurred under sulfide-undersaturated conditions. These observations are critical as sulfur in MORBs is often lost by degassing during eruption (e.g., Alt and Shanks, 2011). This can be also the case for the Kane Megamullion MORBs as suggested by increasing Cl/S ratio upon cooling (Fig. DR1; cf. Lesne et al., 2011).

In a correlation matrix of Zn, Cu, Pb, As, Sb and Tl, coefficients of determination between element pairs are all above 0.7 (Table DR5), with the exception of Tl (R^2 =

Publisher: GSA
Journal: GEOL: Geology
DOI:10.1130/G39287.1

0.24–0.52). These strong correlations imply that the chalcophile element contents are controlled by a common parameter. In the absence of sulfide this parameter is likely element partitioning between melt and clinopyroxene, where $D_{Ni} > D_{Ga} > D_{Zn} > D_{Cu} > D_{Sb}$ (Fig. 3; Jochum et al., 2011). Indeed, Ni/Ga, Ga/Zn, Zn/Cu and Cu/Sb all fall with decreasing Mg# in our basalts. Ni/Ga falls from 7.8 to 5.9 ($R^2 = 0.92$), and the others from 0.20 to 0.15 ($R^2 = 0.90$), from 1.3 to 1.0 ($R^2 = 0.72$) and from 309 to 72 ($R^2 = 0.83$), respectively. Therefore, the Sb concentration in the most evolved Kane Megamullion MORBs is ~15 times larger than the initial Sb concentration at 8.3 MgO wt.%. In contrast, Cu, Zn, and Ga concentrations increase more modestly, and Ni decreases (Fig. 3).

DISCUSSION

Data summarized on Figures 1-3 is consistent with Kane Megamullion MORBs having evolved by low-pressure fractional crystallization under sulfide-undersaturated conditions, and with other MORBs from the Kane area (22–25°N, Fig. DR2; Bryan et al., 1981). Differentiation of chalcophile elements under sulfide-undersaturated conditions is known from plume-related MORBs of Jenner and O'Neill (2012). The plume-related MORBs differ, however, from the Kane Megamullion MORBs by their elevated Cu contents, with Cu_8 (Cu content at 8 wt.% MgO) ranging from 130 to160 ppm.

In principle, Cu-poor MORBs could be derived from a sulfide-poor mantle (Fig. 1: Model A). A primitive melt with only 25 ppm Cu formed at a typical degree of mantle partial melting at the Kane Megamullion (11%–14%; Dick et al., 2010) would require a mantle source with ~8 ppm Cu at 1.8 GPa or ~12 ppm Cu at 4.5 GPa (Lee et al., 2012). Cu-poor depleted mantle is known for example from the Finero orogenic peridotites with

Publisher: GSA
Journal: GEOL: Geology
DOI:10.1130/G39287.1

7 ppm average Cu (Garuti et al., 1984). At Kane Megamullion, however, Cu-poor mantle is unrealistic as spinel harzburgites there contain on average 28 ppm Cu (Table DR6).

Assuming that a typical mantle source with ~30 ppm Cu produces primitive basalt melts with ~120 ppm Cu (Lee et al., 2012; Fig. 1), an initial depletion process driving Cu concentrations from 120 to 60 ppm Cu is required. We thus propose an alternative model involving two steps of magmatic differentiation (Fig. 1: Model B; Fig. 4). In the first step, chalcophile elements are removed from the melt during its ascent through the mantle (orange color in Figures 1 and 4). The second step is exactly the same as in model A, with low-pressure sulfide-undersaturated fractional crystallization in the crust (red color in Figures 1 and 4).

We propose that melt-mantle reaction is the differentiation mechanism that drove the chalcophile elements concentrations to low levels during the first step. The Kane Megamullion dunites, plagioclase harzburgites, and mantle-gabbro contacts, which all interacted with MORB-like melt (Dick et al., 2010), contain enhanced Cu concentrations (57–230, 90–209, up to 305 ppm, respectively). Sulfides have been found in mantle samples from a variety of other settings that underwent melt-rock reaction, including in mantle xenoliths (Lorand et al., 2003; Wang et al., 2009; Chen et al., 2014), orogenic mantle sections (Rehkämper et al., 1999; Lorand et al., 1993) abyssal peridotites (Rehkämper et al., 1999; Lorand et al., 1993) and potentially slow-spreading ridge ophiolites (Madrigal et al. 2015; Schwarzenbach et al., 2016). Such an enrichment of mantle in various elements, including chalcophile elements, due to melt-mantle reaction is called refertilization (e.g., Niu, 2004).

Publisher: GSA
Journal: GEOL: Geology
DOI:10.1130/G39287.1

The mechanism of sulfide crystallization from a melt interacting with mantle has not yet been fully explained. The aforementioned broad spectrum of tectonic settings, encompassing a wide range of temperatures and pressures, suggests that neither temperature nor pressure is crucial for controlling the refertilization of mantle by chalcophile elements. The difference in Fe content between a melt and the mantle, though, could be a common factor for all the settings and trigger sulfide crystallization during mantle-melt reaction. The sulfur concentration at sulfide saturation (SCSS) strongly decreases with the decreasing iron content of the melt, especially in the range of 5–15 wt.% FeO (O'Neill and Mavrogenes, 2002; Haughton et al., 1974; Ariskin et al., 2013). The FeO content in average MORB is ~10.5 wt.% (Gale et al., 2013), and FeO_8 (the FeO content at an MgO value of 8 wt.%) for the Kane Megamullion MORB is 10.6 wt.% FeO (Table DR1). By contrast, the average mantle peridotite contains 8.0 wt.% FeO (Lyubetskaya and Korenaga, 2007), and the median FeO content in the Kane Megamullion spinel harzburgites is 7.6 wt.%. Based on the model of Ariskin et al. (2013), SCSS should fall from 1500 to 900 ppm if FeO content of a melt would decrease from 10.6 to 7.6 wt.% FeO. A further drop of SCSS is expected by increasing the Ni content of the melt (Ariskin et al., 2013). Fe and Ni in melt are buffered by the exchange reaction with large amount of olivine on the conduit walls that causes Fe loss (Dick and Natland, 1996; Falloon et al., 2001) and Ni gain (Hart and Davis, 1978) in the melt, both of which could lead to sulfide crystallization. The Fe loss causing sulfide crystallization could also be achieved by simple olivine or spinel crystallization as proposed by Luguet and Lorand (1999) and Luguet et al. (2003). Both would, however, trigger a simultaneous Ni loss, which could possibly cancel the effect of Fe loss.

Publisher: GSA
Journal: GEOL: Geology
DOI:10.1130/G39287.1

Refertilization of the mantle with sulfides is only moderate in most of the tectonic settings listed above. For example, typical refertilized orogenic mantle contains a moderately elevated Cu concentrations of ~50 ppm Cu (Lorand et al., 2013), whereas the Cu content of the Kane Megamullion re-fertilized mantle is enhanced up to ~300 ppm. This excessive enrichment and the accompanied depletion of Kane Megamullion MORBs thus seem to be setting-specific, and linked to the very thin crust and the shallow mantle in the area. The additional conductive cooling brought by hydrothermal circulation in this ultrashallow mantle accelerates melt solidification upon reaction with the mantle (Fig. 4). In addition, hydrothermal circulation introduces high amounts (up to ~15 wt.%, Table DR7) of water into the shallow mantle. High water content of the Kane Megamullion MORBs (up to 1.8 wt.% in glass, and up to 2.7 wt.% in bulk-rocks), and possible crystallization of clinopyroxene before plagioclase (Fig. 3, cf. Danyushevsky, 2001) may indicate that the water was partially stored in the altered peridotite already before mantle-melt reaction. We have documented contact metamorphism along the recovered serpentinite-gabbro contacts at the Kane Megamullion, which suggests the melt-serpentinite reaction in fact takes place (Fig. DR3). The water lowers the solidus temperature of the melt-mantle reaction allowing a yet larger amount of melt to react with the conduit walls, and yet more efficient FeO loss. Consequently, sub-crustal sulfide crystallization from the Kane Megamullion MORBs can be excessive with respect to MORBs erupted on a completely developed oceanic crust.

CONCLUSIONS

MORBs at slow and ultraslow-spreading ridges with low magma supply rates may become sulfide-undersaturated due to extensive sub-crustal sulfide crystallization

following melt reaction with the mantle. The crystallization of sulfides during melt-mantle reaction could be achieved by lowering the level of sulfide concentration at sulfide saturation in the portion of melt that was depleted in FeO. This process may be global, but it becomes increasingly significant at ridge segments with thin crust, where the melt-mantle reaction can proceed to very shallow depths. In addition, conductive cooling related to hydrothermal circulation and high water content of the serpentinized peridotite boost the intensity of the melt-rock reaction.

ACKNOWLEDGMENTS

We thank editor Brendan Murphy, Claude Herzberg, John Mavrogenes, and an anonymous reviewer for their thorough and insightful comments. In addition, we would like to acknowledge D. Neave, F. Ridolfi, J. Feige, C. Zhang, F. Holtz, and L. Kirchhoff from the Leibniz Universität Hannover, and M. Ciążela, J. Nowak and A. Żelaźniewicz from the Polish Academy of Sciences. This research was funded by a Diamond Grant of the Polish Ministry of Science and Higher Education (DI2012 2057 42 to Ciazela), and partially supported by the European Association of Geochemistry (Early Career Science Ambassador grant to Ciazela) and the National Science Foundation (grant #'s OCE1434452 and OCE1637130 to Dick).

REFERENCES CITED

Alt, J.C., and Shanks, W.C., 2011, Microbial sulfate reduction and the sulfur budget for a complete section of altered oceanic basalts, IODP Hole 1256D (eastern Pacific): Earth and Planetary Science Letters, v. 310, p. 73–83, doi:10.1016/j.epsl.2011.07.027.

Ariskin, A.A., Danyushevsky, L.V., Bychkov, K.A., McNeill, A.W., Barmina, G.S., and Nikolaev, G.S., 2013, Modeling solubility of Fe-Ni sulfides in basaltic magmas: The effect of nickel: Economic Geology and the Bulletin of the Society of Economic Geologists, v. 108, p. 1983–2003, doi:10.2113/econgeo.108.8.1983.

Bryan, W.B., Thompson, G., and Ludden, J.N., 1981, Compositional variation in normal MORB from 22°-25° N; Mid-Atlantic Ridge and Kane Fracture Zone: Journal of Geophysical Research, v. 86, p. 11815–11836, doi:10.1029/JB086iB12p11815.

Cann, J.R., Blackmann, D.K., Smith, D.K., McAllister, E., Janssen, B., Mello, S., Avgerinos, E., Pascoe, A.R., and Escartin, J., 1997, Corrugated slip surfaces formed at ridge-transform intersections on the Mid-Atlantic Ridge: Nature, v. 385, p. 329–332, doi:10.1038/385329a0.

Cannat, M., Mevel, C., Maia, M., Deplus, C., Durand, C., Gente, P., Agrinier, P., Belarouchi, A., Dubuisson, G., Humler, E., and Reynolds, J.R., 1995, Thin crust, ultramafic exposures, and rugged faulting patterns at the Mid-Atlantic Ridge (22°-24°N): Geology, v. 23, p. 49–52, doi:10.1130/0091-7613(1995)023<0049:TCUEAR>2.3.CO;2.

Chen, M.-M., Tian, W., Suzuki, K., Tejada, M.-L.-G., Liu, F.-L., Senda, R., Wei, C.-J., Chen, B., and Chu, Z.-Y., 2014, Peridotite and pyroxenite xenoliths from Tarim, NW China: Evidences for melt depletion and mantle refertilization in the mantle source region of the Tarim flood basalt: Lithos, v. 204, p. 97–111, doi:10.1016/j.lithos.2014.01.005.

Coogan, L.A., 2014, The lower oceanic crust, *in* Rudnick, R.L., ed., The Crust, Vol. 4, Treatise on Geochemistry, Second Edition (Holland, H.D., and Turekian, K.K., eds.): New York, Elsevier, p. 497–541, doi:10.1016/B978-0-08-095975-7.00316-8.

Crisp, J.A., 1984, Rates of magma emplacement and volcanic output: Journal of Volcanology and Geothermal Research, v. 20, p. 177–211, doi:10.1016/0377-0273(84)90039-8.

Danyushevsky, L.V., 2001, The effect of small amounts of H2O on crystallisation of mid-ocean ridge and backarc basin magmas: Journal of Volcanology and Geothermal Research, v. 110, p. 265–280, doi:10.1016/S0377-0273(01)00213-X.

Dick, H.J.B., Lissenberg, C.J., and Warren, J.M., 2010, Mantle Melting, Melt Transport, and Delivery Beneath a Slow-Spreading Ridge: The Paleo-MAR from 23 15‘N to 23 45’N: Journal of Petrology, v. 51, p. 425–467, doi:10.1093/petrology/egp088.

Dick, H.J.B., and Natland, J.H., 1996, Late-stage melt evolution and transport in the shallow mantle beneath the East Pacific Rise: Proceedings of the Ocean Drilling Program. Scientific Results, v. 147, p. 103–134.

Dick, H.J.B., Tivey, M., and Tucholke, B.E., 2008, Plutonic foundation of a slow-spreading ridge segment: Oceanic core complex at Kane Megamullion, 23°30′N, 45°20′W: Geochemistry Geophysics Geosystems, v. 9, Q05014, doi:10.1029/2007GC001645.

Falloon, T.J., Danyushevsky, L. V., and Green, D.H., 2001, Peridotite Melting at 1 GPa: Reversal Experiments on Partial Melt Compositions Produced by Peridotite-Basalt Sandwich Experiments: Journal of Petrology, v. 42, p. 2363–2390, doi: 10.1093/petrology/42.12.2363.

Francis, R.D., 1990, Sulfide globules in mid-ocean ridge basalts (MORB), and the effect of oxygen abundance in FeSO liquids on the ability of those liquids to partition metals from MORB and komatiite magmas: Chemical Geology, v. 85, p. 199–213, doi:10.1016/0009-2541(90)90001-N.

Gale, A., Dalton, C.A., Langmuir, C.H., Su, Y., and Schilling, J.G., 2013, The mean composition of ocean ridge basalts: Geochemistry Geophysics Geosystems, v. 14, p. 489–518, doi:10.1029/2012GC004334.

Garuti, G., Gorgoni, C., and Sighinolfi, G.P., 1984, Sulfide mineralogy and chalcophile and siderophile element abundances in the Ivrea-Verbano mantle peridotites (Western Italian Alps): Earth and Planetary Science Letters, v. 70, p. 69–87, doi:10.1016/0012-821X(84)90210-3.

Hart, S.R., and Davis, K.E., 1978, Nickel partitioning between olivine and silicate melt: Earth and Planetary Science Letters, v. 40, p. 203–219, doi:10.1016/0012-821X(78)90091-2.

Haughton, D.R., Roeder, P.L., and Skinner, B.J., 1974, Solubility of sulfur in mafic magmas: Economic Geology and the Bulletin of the Society of Economic Geologists, v. 69, p. 451–467, doi:10.2113/gsecongeo.69.4.451.

Herzberg, C., 2004, Partial crystallization of mid-ocean ridge basalts in the crust and mantle: Journal of Petrology, v. 45, p. 2389–2405, doi:10.1093/petrology/egh040.

Jenner, F.E., and O'Neill, H.S.C., 2012, Analysis of 60 elements in 616 ocean floor basaltic glasses: Geochemistry Geophysics Geosystems, v. 13, Q02005, doi:10.1029/2011GC004009.

Jochum, K.P., Weis, U., Stoll, B., Kuzmin, D., Yang, Q., Raczek, I., Jacob, D.E., Stracke, A., Birbaum, K., Frick, D.A., Günther, D., and Enzweiler, J., 2011, Determination of Reference Values for NIST SRM 610–617 Glasses Following ISO Guidelines: Geostandards and Geoanalytical Research, v. 35, p. 397–429, doi:10.1111/j.1751-908X.2011.00120.x.

Klein, E.M., and Langmuir, C.H., 1987, Global Correlations of Ocean Ridge Basalt Chemistry with Axial Depth and Crustal Thickness: Journal of Geophysical Research, v. 92, p. 8089–8115, doi:10.1029/JB092iB08p08089.

Lee, C.-T., Luffi, P., Chin, E.J., Bouchet, R., Dasgupta, R., Morton, D.M., Le Roux, V., Yin, Q., and Jin, D., 2012, Copper systematics in arc magmas and implications for crust-mantle differentiation: Science, v. 336, p. 64–68, doi:10.1126/science.1217313.

Lesne, P., Kohn, S.C., Blundy, J., Witham, F., Botcharnikov, R.E., and Behrens, H., 2011, Experimental simulation of closed-system degassing in the system basalt-H2O–CO2-S-Cl: Journal of Petrology, v. 52, p. 1737–1762, doi:10.1093/petrology/egr027.

Lissner, M., König, S., Luguet, A., le Roux, P.J., Schuth, S., Heuser, A., and le Roex, A.P., 2014, Selenium and tellurium systematics in MORBs from the southern Mid-Atlantic Ridge (47–50°S): Geochimica et Cosmochimica Acta, v. 144, p. 379–402, doi:10.1016/j.gca.2014.08.023.

Lorand, J.P., Keays, R.R., and Bodinier, J.L., 1993, Copper and noble metal enrichments across the lithosphere-asthenosphere boundary of mantle diapirs: Evidence from the lanzo lherzolite massif: Journal of Petrology, v. 34, p. 1111–1140, doi:10.1093/petrology/34.6.1111.

Lorand, J.-P., Luguet, A., and Alard, O., 2013, Platinum-group element systematics and petrogenetic processing of the continental upper mantle: A review: Lithos, v. 164–167, p. 2–21, doi:10.1016/j.lithos.2012.08.017.

Lorand, J.P., Reisberg, L., and Bedini, R.M., 2003, Platinum-group elements and melt percolation processes in Sidamo spinel peridotite xenoliths, Ethiopia, East African Rift: Chemical Geology, v. 196, p. 57–75, doi:10.1016/S0009-2541(02)00407-2.

Luguet, A., and Lorand, J., 1999, Fe-Ni-Cu sulphides of abyssal peridotites from the MARK area (Mid-Atlantic ridge, 20–24°N): Geomaterials, v. 329, p. 637–644.

Luguet, A., Lorand, J.-P., and Seyler, M., 2003, Sulfide petrology and highly siderophile element geochemistry of abyssal peridotites: a coupled study of samples from the Kane Fracture Zone (45°W 23°20N, MARK area, Atlantic Ocean): Geochimica et Cosmochimica Acta, v. 67, p. 1553–1570, doi:10.1016/S0016-7037(02)01133-X.

Lyubetskaya, T., and Korenaga, J., 2007, Chemical composition of Earth's primitive mantle and its variance: 1. Method and results: Journal of Geophysical Research, v. 112, p. B03211, doi:10.1029/2005JB004223.

Madrigal, P., Gazel, E., Denyer, P., Smith, I., Jicha, B., Flores, K.E., Coleman, D., and Snow, J., 2015, A melt-focusing zone in the lithospheric mantle preserved in the Santa Elena Ophiolite, Costa Rica: Lithos, v. 230, p. 189–205, doi: 10.1016/j.lithos.2015.04.015.

Niu, Y., 2004, Bulk-rock major and trace element compositions of abyssal peridotites: Implications for mantle melting, melt extraction and post-melting processes beneath Mid-Ocean ridges: Journal of Petrology, v. 45, p. 2423–2458, doi:10.1093/petrology/egh068.

O'Neill, H.S.C., and Mavrogenes, J.A., 2002, The Sulfide Capacity and the Sulfur Content at Sulfide Saturation of Silicate Melts at 1400°C and 1 bar: Journal of Petrology, v. 43, p. 1049–1087, doi:10.1093/petrology/43.6.1049.

Rehkämper, M., Halliday, A.N., Alt, J., Fitton, J.G., Zipfel, J., and Takazawa, E., 1999, Non-chondritic platinum-group element ratios in oceanic mantle lithosphere: Petrogenetic signature of melt percolation?: Earth and Planetary Science Letters, v. 172, p. 65–81, doi:10.1016/S0012-821X(99)00193-4.

Schwarzenbach, E.M., Gill, B.C., Gazel, E., and Madrigal, P., 2016, Sulfur and carbon geochemistry of the Santa Elena peridotites: Comparing oceanic and continental processes during peridotite alteration: Lithos, v. 252-253, p. 92–108, doi: 10.1016/j.lithos.2016.02.017

Tucholke, B.E., Lin, J., and Kleinrock, M.C., 1998, Megamullions and mullion structure defining oceanic metamorphic core complexes on the Mid-Atlantic Ridge: Journal of Geophysical Research, v. 103, p. 9857–9866, doi:10.1029/98JB00167.

Villiger, S., Müntener, O., and Ulmer, P., 2007, Crystallization pressures of mid-ocean ridge basalts derived from major element variations of glasses from equilibrium and fractional crystallization experiments: Journal of Geophysical Research. Solid Earth, v. 112, p. 1–18, doi:10.1029/2006JB004342.

Wang, K.L., O'Reilly, S.Y., Griffin, W.L., Pearson, N.J., and Zhang, M., 2009, Sulfides in mantle peridotites from Penghu Islands, Taiwan: Melt percolation, PGE fractionation, and the lithospheric evolution of the South China block: Geochimica et Cosmochimica Acta, v. 73, p. 4531–4557, doi:10.1016/j.gca.2009.04.030.

White, W.M., and Klein, E.M., 2013, Composition of the Oceanic Crust, *in* Rudnick, R.L., ed., The Crust, Vol. 4, Treatise on Geochemistry, Second Edition (Holland, H.D., and Turekian, K.K., eds.): Oxford, UK, Elsevier, p. 457–496, doi:10.1016/B978-0-08-095975-7.00315-6.

FIGURE CAPTIONS

Figure 1. Cu versus MgO contents of the Kane Megamullion MORBs (red) compared to non-plume-related MORBs from the reference data set of Jenner and O'Neill (2012; gray). Models A and B are two possible scenarios for the early MORB differentiation (see Discussion). Modified after Jenner and O'Neill, 2012.

Figure 2. Chalcophile element versus MgO contents of the Kane Megamullion MORBs.

Figure 3. Ratios of actual to initial (for MgO wt.% = 8.3) chalcophile element contents versus MgO contents of the Kane Megamullion MORBs. Note that element concentrations grow proportionally fast to the decreasing clinopyroxene-melt partition coefficients (D_{cpx}), which are <0.02 for Sb, 0.07–0.36 for Cu, 0.41–0.50 for Zn, 0.74 for Ga, and 2.6–4.4 for Ni (Jochum et al., 2011).

Figure 4. Lithosphere profile in the Kane area as proposed by Cannat et al. (1995) along with the Cu concentration observed in the Kane Megamullion basalts (red) and the

predicted Cu concentrations at the first stage of differentiation (orange). Modified after Dick et al., 2006.

1GSA Data Repository item 2017xxx, xxxxxxxx, is available online at http://www.geosociety.org/datarepository/2017/ or on request from editing@geosociety.org.

Figure 1

Click here to download Figure Fig1.tif

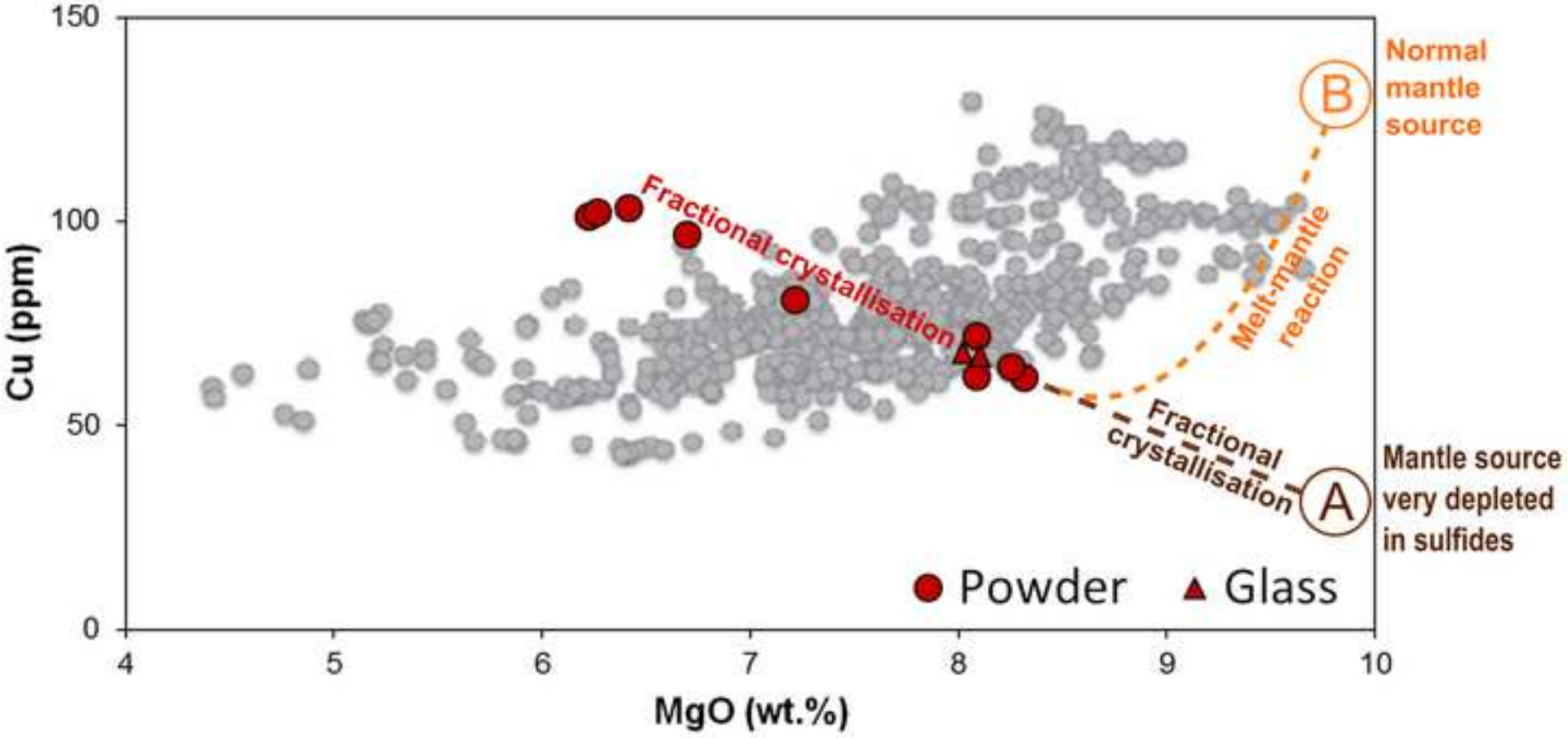

Figure 2

Click here to download Figure Fig2.tif

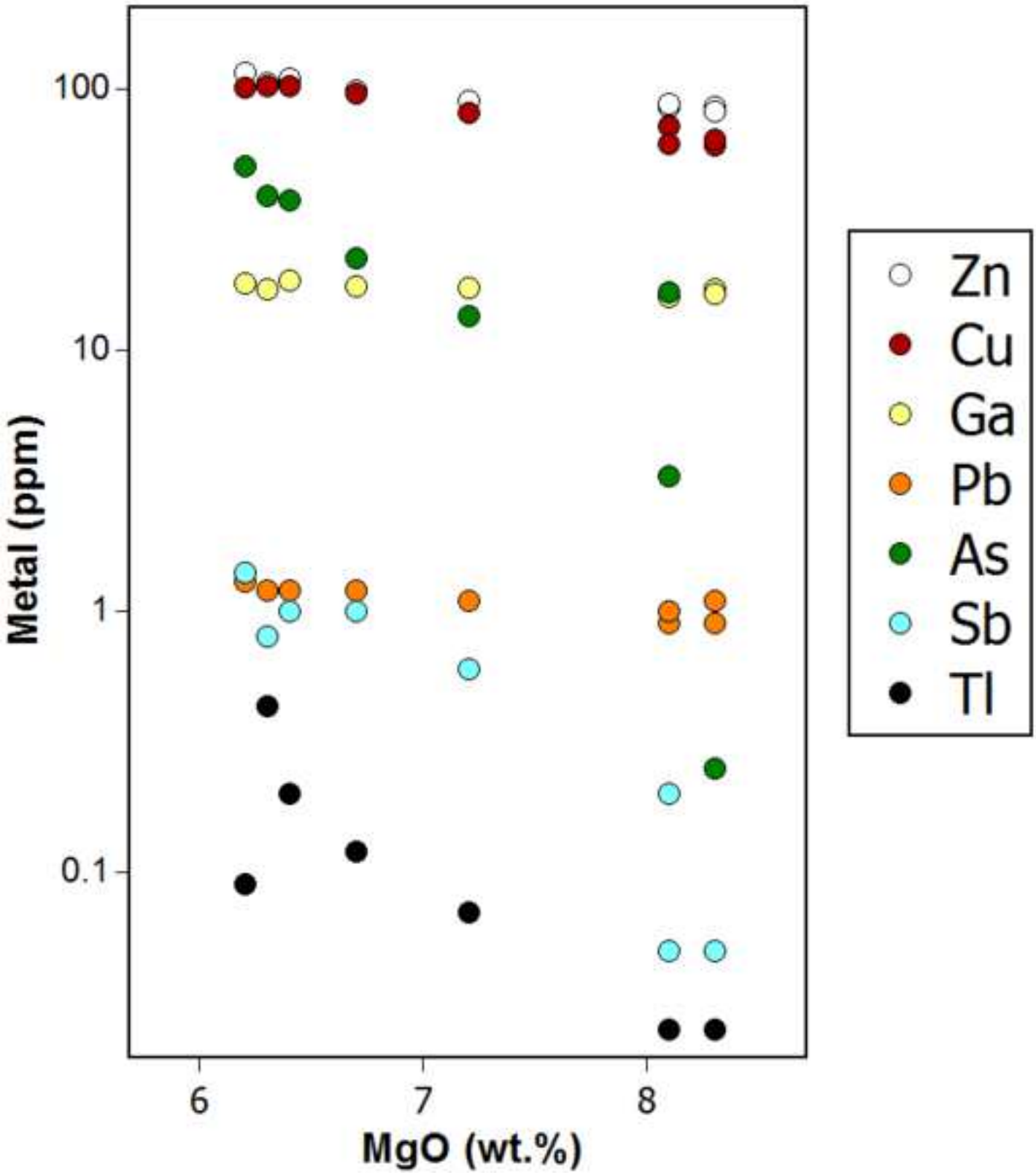

Figure 3

Click here to download Figure Fig3.tif

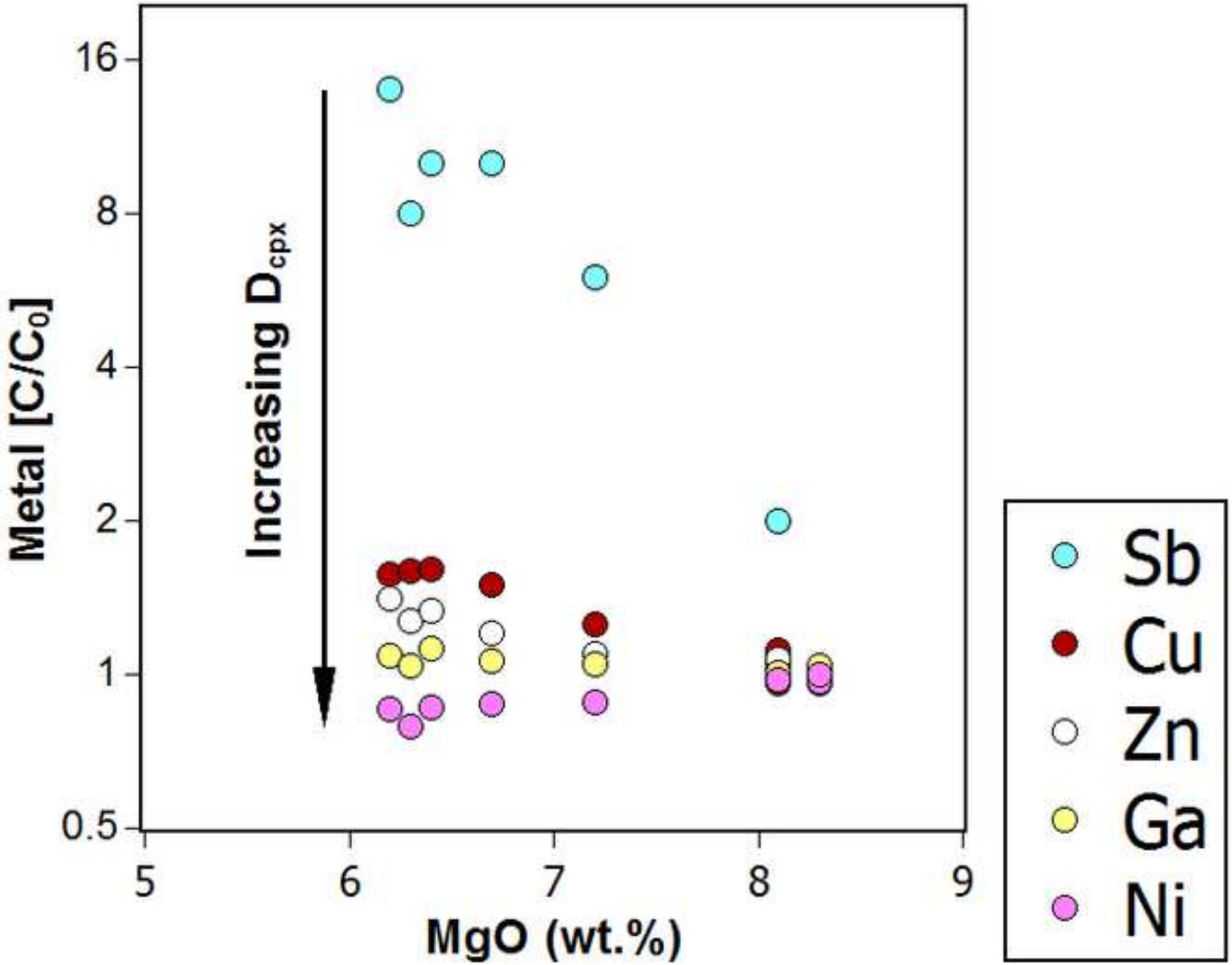

Figure 4

Click here to download Figure Fig4.tif

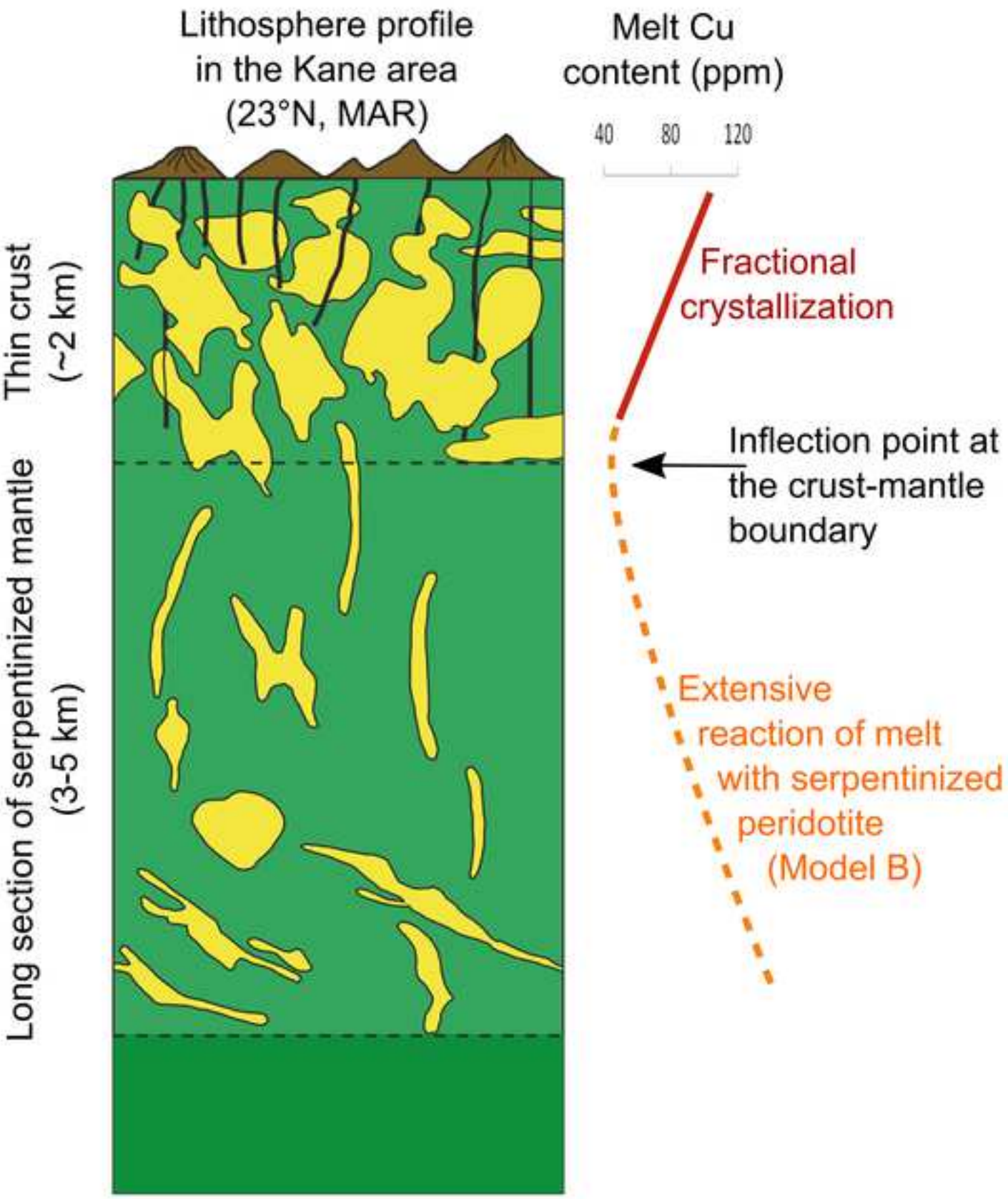

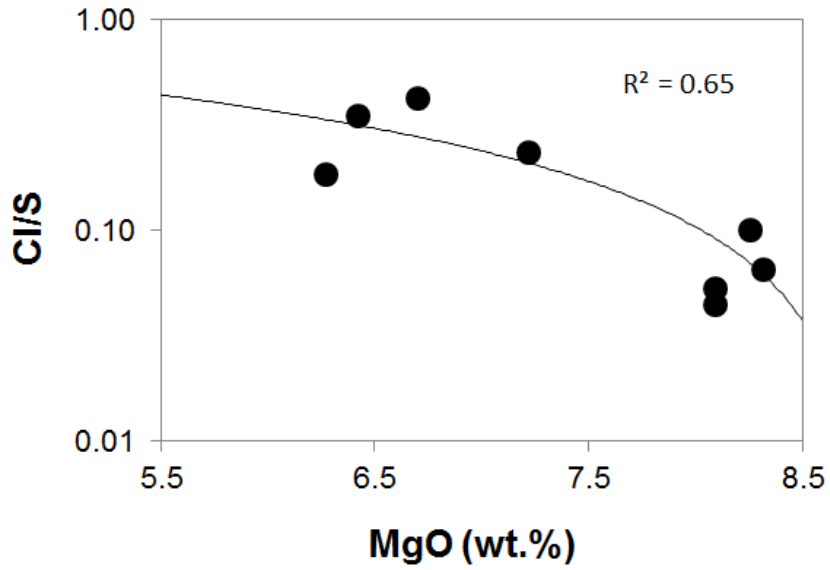

Figure DR1. Bulk-rock Cl/S ratios versus bulk-rock contents of MgO in the Kane Megamullion MORBs.

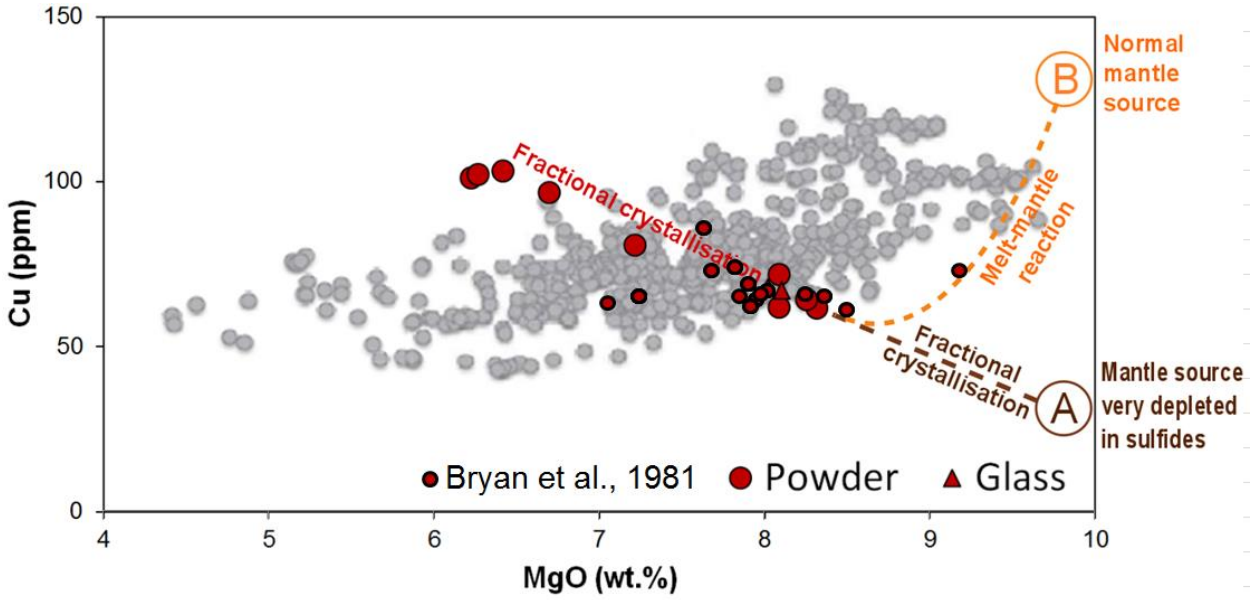

Figure DR2. Bulk-rock copper content versus bulk-rock MgO in the Mid Atlantic Ridge Kane MORB's (22-25°N, Bryan et al., 1981) plotted on top of Figure 1.

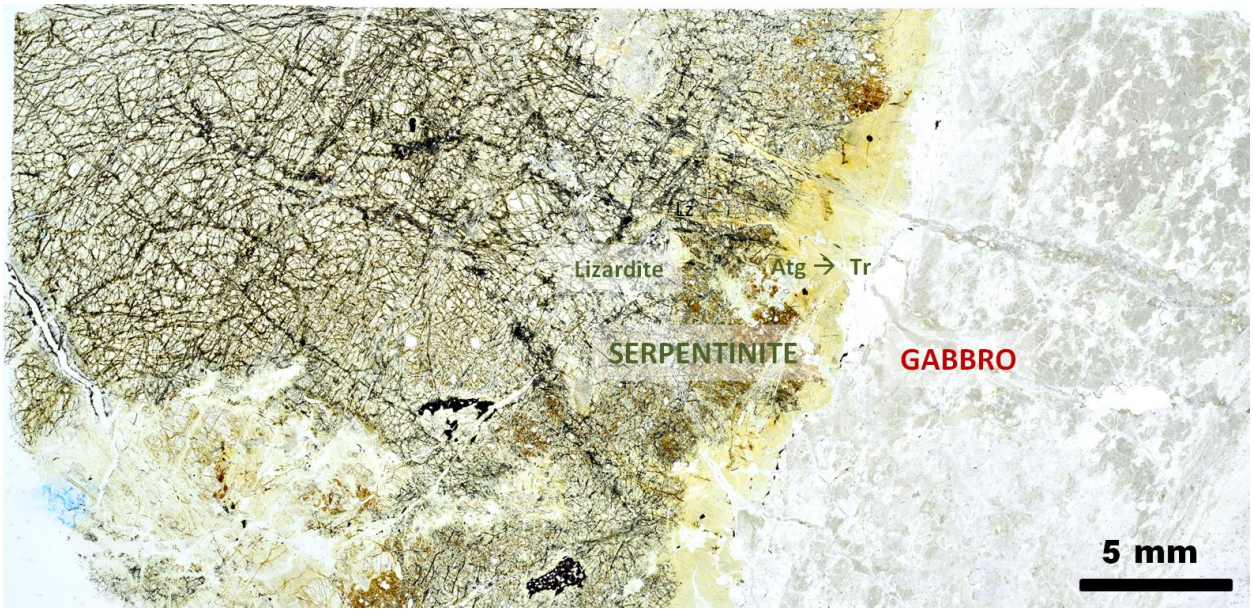

Figure DR3. Thin-section microphotography of a serpentinite-gabbro contact with a distinct zone of contact metamorphism (yellow) between the serpentinite host rock and the gabbro vein. Sample 21-9. Plane-polarized transmitted light. Atg, Antigorite. Tr, Tremolite.

Table DR1. Major and trace element composition of MORBs from the Kane Megamullion OCC

Sample	1-2	110-1	110-2	111-2	111-3	111-4	111-7	111-16	111-17
Mg#	0.51	0.53	0.55	0.54	0.61	0.57	0.60	0.61	0.60
major elements (wt.%)									
SiO_2	46.3	46.6	47.8	47.4	49.0	48.1	49.0	49.4	47.8
TiO_2	1.76	1.64	1.59	1.65	1.58	1.64	1.57	1.55	1.62
Al_2O_3	17.2	16.4	15.9	16.4	15.7	16.0	15.6	15.6	16.1
Fe_2O_3	11.7	11.0	10.6	10.9	10.6	10.7	10.5	10.4	10.8
MnO	0.17	0.19	0.18	0.16	0.18	0.18	0.18	0.18	0.18
MgO	6.23	6.27	6.70	6.42	8.32	7.22	8.09	8.26	8.09
CaO	11.5	11.4	11.1	11.2	11.2	11.5	11.0	11.1	11.4
Na_2O	2.94	3.02	3.03	3.08	2.71	2.83	2.79	2.74	2.78
K_2O	0.09	0.18	0.17	0.16	0.14	0.26	0.20	0.16	0.12
P_2O_5	0.33	0.32	0.22	0.28	0.14	0.21	0.15	0.15	0.22
L.O.I.	1.6	2.7	2.5	2.1	0.1	1.0	0.4	0.1	0.5
Total	99.7	99.8	99.8	99.8	99.6	99.7	99.6	99.6	99.7
Chalcophile elements (ppm)									
Cu	101	102	96	103	61	81	72	64	62
As	50	39	23	37	-	14	3	-	17
Zn	116	105	99	110	85	90	86	82	88
Ga	17.9	17.2	17.6	18.5	17.2	17.3	16.6	16.5	16.1
Pb	1.3	1.2	1.2	1.2	0.9	1.1	0.9	1.1	1.0
Se	2	1.7	1.7	1.8	2.1	2	2.2	1.3	2.3
Sb	1.4	0.8	1.0	1.0	-	0.6	-	-	0.2
Tl	0.09	0.43	0.12	0.20	-	0.07	-	-	-
Ni	110	102	113	111	125	114	126	129	126
Ag	0.06	-	0.07	-	-	0.07	-	0.24	0.07
Bi	-	-	0.03	-	-	-	0.02	0.11	0.02
Cd	0.2	0.3	0.2	0.2	0.1	0.2	0.2	0.2	0.2
Te	-	0.4	-	-	-	-	0.2	0.2	0.2
Hg	30	10	-	-	-	20	-	10	10
Ge	0.2	0.6	0.3	0.3	0.2	0.5	0.2	0.2	0.3

LOI - loss-on-ignition

The estimates of analytical precision (1 SD) are as follows: Cu, ±1.5%; Cd, ±33.3%; Ge, ±7.1%; Ga, ±1.5%; Pb, ±7.1%; Tl, ±1.5%; major elements ±1-2%, and were determined by repeated measurements of unknown samples. The estimates of analytical accuracy are as follows: As, ±3.7%; Cu, ±5.3%; Cd, ±14.6%; Ge, ±7.1%; Ga, ±17.0%; Hg, ±31.3%; Pb, ±4.5%; Sb, ±5.3%; Te, ±11.7%; Tl, ±10.6% and were determined by measurements of variuos certified material (GXR-1, GXR-4, GXR-6, SDC-1, SAR-M (U.S.G.S), DNC, SBC-1, DMMAS).

Table DR2. Major and trace element composition of olivines from the Kane Megamullion MORBs

Sample	1-2		110-1		110-2		111-2		111-3		111-4		111-7		111-16		111-17	
n	5	SD	5	SD	8	SD	7	SD	4	SD	6	SD	8	SD	4	SD	7	SD
major elements (wt%)																		
SiO_2	39.8	0.4	39.9	0.1	40.0	0.3	40.1	0.1	40.0	0.5	39.9	0.3	40.1	0.3	40.2	0.3	39.8	0.4
Al_2O_3	0.01	0.02	0.02	0.04	0.0	0.0	0.04	0.05	0.07	0.08	0.02	0.04	0.01	0.04	0.14	0.15	0.17	0.17
TiO_2	0.02	0.04	0.0	0.0	0.0	0.0	0.01	0.02	0.0	0.0	0.0	0.0	0.01	0.04	0.04	0.05	0.06	0.05
CaO	0.32	0.04	0.3	0.0	0.33	0.05	0.32	0.03	0.31	0.04	0.3	0.0	0.36	0.05	0.4	0.1	0.4	0.1
FeO	13.7	0.7	13.4	0.2	13.2	0.3	13.5	0.3	13.7	0.8	13.4	0.3	14.0	0.4	13.5	0.4	14.1	1.1
MnO	0.2	0.1	0.23	0.01	0.2	0.1	0.2	0.1	0.1	0.1	0.25	0.02	0.1	0.1	0.21	0.04	0.2	0.2
MgO	45.9	0.8	46.2	0.3	46.6	0.2	46.6	0.3	45.4	0.6	45.4	0.2	45.1	0.4	44.8	0.6	45.0	1.3
NiO	0.22	0.02	0.220	0.003	0.210	0.007	0.210	0.008	0.21	0.02	0.22	0.01	0.15	0.02	0.21	0.02	0.19	0.03
Cr_2O_3	0.04	0.06	0.0	0.0	0.0	0.0	0.02	0.05	0.0	0.0	0.0	0.0	0.0	0.0	0.03	0.06	0.04	0.06
Total		100.0		100.0		100.4		100.8		99.6		99.3		99.8		99.4		99.7
Fo (%)		85.1		85.5		85.7		85.5		85.1		85.2		84.7		84.9		84.4
trace elements (μg/g)																		
Co (59)	148	15	168	1	164	7	157	6	160	13	162	4	130	18	155	6	140	12
Ni (60, 61, 62)	1747	163	1771	22	1683	59	1656	64	1653	183	1731	101	1217	179	1680	137	1502	271
Cu (63)	14	13	7	8	4	4	11	8	10	13	3	3	22	16	23	5	34	20
Zn (67)	92	20	80	7	68	8	73	7	95	7	79	3	82	20	98	19	78	15
Ga (71)	0.6	0.3	0.16	0.04	0.17	0.05	0.20	0.08	0.5	0.7	0.3	0.4	1.8	1.1	0.9	0.5	1.5	1.6
Ge (74)	3.19	-	1.18	0.08	1.19	0.09	1.14	0.09	1.22	0.02	1.2	0.1	1.3	0.1	-	-	-	-
As (75)	-	-	1.9	2.5	1.2	2.5	3.6	3.8	0.2	0.1	0.1	0.0	0.5	0.1	-	-	1.9	0.1
Se (77)	-	-	4.7	0.3	5.4	0.7	5.0	0.4	4.0	0.6	4.3	0.3	4.0	0.5	-	-	-	-
Pd (106)	0.014	-	0.004	0.003	0.004	0.002	0.003	0.000	0.004	0.002	0.003	0.001	0.005	0.002	-	-	-	-
Cd (111)	-	-	0.021	0.004	0.023	0.004	-	-	0.03	0.01	-	-	0.051	0.009	-	-	-	-
In (115)	-	-	0.028	0.001	0.022	0.002	0.025	0.002	0.016	0.006	0.024	0.004	0.027	0.008	-	-	-	-
Sn (118)	2.1	0.8	5.8	0.3	4.6	0.2	5.4	0.6	2.2	1.0	4.4	0.3	2.7	1.1	3.1	1.5	3.9	0.3
Sb (121)	-	-	0.20	0.09	-	-	0.09	-	0.12	0.05	-	-	-	-	-	-	-	-
Te (125)	-	-	0.08	0.03	0.08	0.03	0.09	-	0.09	-	-	-	-	-	-	-	-	-
Pt (195)	5.7	9.5	1.6	2.3	1.0	1.2	0.9	0.9	2.8	2.7	1.0	1.6	1.1	0.5	4.5	3.4	6.6	8.1
Au (197)	1.1	-	0.11	0.09	0.09	0.04	-	-	0.11	0.06	-	-	0.1	-	0.4	-	0.4	-
Pb (206, 208)	0.9	0.8	0.3	0.3	0.5	0.7	1.0	0.7	0.8	0.5	0.11	0.06	1.4	0.6	1.6	1.4	1.2	0.4
Bi (209)	-	-	0.005	0.002	0.04	0.06	0.08	0.07	0.02	0.02	-	-	0.06	0.04	-	-	0.034	0.003

Fo=100*(molar Mg/(Mg+Fe+Ca+Mn)); NiO was determined using LA-ICPMS; SD - standard deviation

Table DR3. Major and trace element composition of plagioclase from the Kane Megamullion MORBs

Sample		1-2		110-1		110-2		111-2		111-3		111-4		111-7		111-16		111-17	
	n	2	SD	3	SD	4	SD	3	SD	5	SD	5	SD	6	SD	2	SD	3	SD
major elements (wt%)																			
SiO_2		53.0	0.4	52.7	1.5	52.5	0.8	54.0	1.0	51.8	0.7	52.0	1.5	51.8	0.4	51.9	0.1	51.6	0.5
Al_2O_3		27.6	0.5	28.8	0.9	28.5	1.4	28.3	0.4	29.4	0.7	28.5	0.7	29.7	0.3	28.8	0.1	28.6	1.0
K_2O		0.2	0.1	0.1	0.0	0.1	0.0	0.1	0.0	0.0	0.0	0.0	0.0	0.0	0.0	0.0	0.0	0.0	0.0
TiO_2		0.2	0.1	0.1	0.1	0.1	0.1	0.1	0.0	0.1	0.0	0.1	0.0	0.1	0.0	0.1	0.0	0.1	0.0
CaO		11.4	1.1	11.9	1.1	12.0	1.5	12.0	0.8	13.7	0.5	12.8	0.9	13.7	0.2	13.2	0.3	13.3	0.5
FeO		1.4	0.4	0.8	0.3	1.4	0.8	1.2	0.1	0.7	0.1	0.8	0.1	0.8	0.1	0.9	0.1	1.1	0.4
MnO		0.0	0.0	0.0	0.0	0.1	0.1	0.0	0.0	0.0	0.0	0.0	0.0	0.0	0.0	0.0	0.0	0.0	0.0
Na_2O		4.5	0.5	4.8	0.5	4.8	0.5	4.8	0.3	3.6	0.3	3.9	0.5	3.7	0.1	3.8	0.1	3.9	0.3
MgO		0.3	0.1	0.1	0.0	0.1	0.1	0.3	0.1	0.3	0.1	0.3	0.1	0.3	0.0	0.4	0.0	0.6	0.4
Total			98.5		99.5		99.4		100.7		99.7		98.5		100.0		99.0		99.3
Or (%)			1.1		0.3		0.4		0.3		0.2		0.3		0.2		0.2		0.2
Ab (%)			41.2		44.9		41.7		41.1		33.0		34.3		32.8		34.2		35.0
An (%)			57.7		54.8		57.9		58.6		66.8		65.5		67.0		65.6		64.7
trace elements (µg/g)																			
Co (59)		13	-	57	77	46	57	19	15	11	7	41	58	6	5	14	18	28	13
Ni (60)		81	-	26	-	75	38	36	15	48	16	45	34	39	32	119	43	135	167
Cu (65)		71	95	42	32	140	90	55	37	61	42	48	18	34	23	87	16	61	24
Zn (66)		54	6	58	10	66	8	64	17	42	26	48	17	44	13	85	8	87	44
Ga (69, 71)		15	1	19.0	0.6	17.0	0.9	18	8	14	2	16.9	0.9	16	2	16.7	1.0	16.3	0.7
Ge (74)		-	-	-	-	1.7	-	-	-	1.6	0.4	1.8	0.1	1.1	-	2.1	-	-	-
As (75)		-	-	18	13	56	37	16	18	0.73	0.06	0.33	0.08	0.5	-	2.39	0.05	0.7	-
Se (77)		-	-	-	-	12	8	-	-	5	2	6.3	0.7	-	-	9.3	-	-	-
In (115)		-	-	-	-	0.11	0.03	-	-	0.063	0.003	0.07	0.01	0.04	-	0.07	0.003	0.06	-
Sn (118)		7	1	6	1	7	1	6	1	5	2	5.5	0.3	3	1	3.6	0.6	5.6	0.8
Pt (195)		0.64	0.09	8.9	-	12	12	3.8	-	2	2	2	2	2	3	3	2	9	7
Tl (203,205)		-	-	-	-	-	-	-	-	0.0215	0.0007	0.05	0.03	0.03	-	0.04	-	-	-
Pb (206,208)		1.1	0.5	2.0	0.7	3	1	2.4	0.5	1.8	0.5	1.3	0.6	1.6	0.8	1.6	0.1	2	-
Bi (209)		-	-	0.07	-	0.11	0.07	0.09	0.03	0.05	0.01	0.020	0.003	0.11	0.09	0.04	-	-	-

Or=100*(molar K/(Ca+Na+K)); Ab=100*(molar Na/ (Ca+Na+K)); An=100*(molar Ca/(Ca+Na+K)); SD - standard deviation

Table DR4. Major and trace element composition of clinopyroxenes from the Kane Megamullion MORBs

Sample	1-2		110-1		110-2		111-2		111-3		111-4	
n	4	SD	8	SD	5	SD	4	SD	5	SD	5	SD
major elements (wt%)												
SiO_2	45.9	0.7	46.4	1.6	48.6	1.2	47.9	0.6	45.4	2.0	47.1	0.5
Al_2O_3	5.9	1.3	5.0	1.0	3.6	0.8	5.3	0.7	6.2	1.9	5.8	0.3
K_2O	0.0	0.0	0.01	0.01	0.0	0.0	0.01	0.02	0.0	0.0	0.01	0.03
TiO_2	3.3	0.3	2.5	0.6	2.1	0.6	2.3	0.2	3.3	0.7	2.5	0.1
CaO	21.1	1.1	19.4	1.0	19.8	0.8	19.7	1.1	20.5	1.0	20.4	0.2
FeO	10.7	1.7	11.9	1.9	10.4	1.4	10.7	0.8	12.3	0.8	8.7	0.8
MnO	0.1	0.1	0.3	0.1	0.3	0.1	0.2	0.2	0.1	0.2	0.20	0.03
Na_2O	0.6	0.2	0.5	0.1	0.5	0.1	0.5	0.2	0.5	0.1	0.4	0.1
MgO	11.2	0.5	12.2	0.9	13.6	1.1	13.2	0.7	10.2	0.7	12.9	0.5
Cr_2O_3	0.04	0.08	0.0	0.0	0.1	0.1	0.2	0.2	0.1	0.1	0.2	0.1
Total		98.9		98.2		99.0		100.0		98.7		98.2
En (%)		37.6		41.3		43.5		42.9		36.0		41.7
Fs (%)		11.3		11.4		10.9		11.1		11.8		10.9
Wo (%)		51.0		47.3		45.6		46.0		52.1		47.4
trace elements (μg/g)												
Co (59)	32	5	54	35	35	5	46	14	37	7	43	8
Ni (60)	84	22	69	33	52	21	158	115	75	50	69	41
Cu (63)	33	16	45	31	28	17	27	8	78	35	33	12
Zn (66)	58	24	94	40	56	12	62	3	124	52	68	12
Ga (69, 71)	14	2	14	3	12	2	10	1	13	1	13	1
Ge (74)	3	-	11	-	3.3	1.0	-	-	3.8	-	3.30	0.04
As (75)	1.4	0.1	19	15	11	6	13	-	1	-	-	-
Pd (106)	0.025	0.006	-	-	0.03	0.01	-	-	-	-	0.02	-
In (115)	0.12	0.01	0.20	0.08	0.19	0.05	-	-	0.17	0.02	0.12	0.02
Sn (118)	6.7	0.7	7	2	5.6	1.0	6.5	-	4.0	0.5	5.0	0.7
Pt (195)	3	5	-	-	8	7	-	-	1.1	0.7	0.2	-
Pb (208)	0.6	0.5	1.8	0.6	2	1	2	1	3	2	0.7	0.2
Bi (209)	-	-	0.4	0.2	0.5	0.6	-	-	0.25	0.05	-	-

En=100*(molar Mg/(Mg+Fe+Ca)); Fs=100*(molar Fe/ (Mg+Fe+Ca)); Wo=100*(molar Ca/(Mg+Fe+Ca)).

SD - standard deviation

Table DR5. Correlation matrix for chalcophile elements of the Kane Megamullion MORBs

	Zn	Cu	Pb	As	Sb	Tl	Ni
Zn	1						
Cu	0.85	1					
Pb	0.71	0.72	1				
As	0.96	0.77	0.72	1			
Sb	0.90	0.85	0.83	0.85	1		
Tl	0.35	0.52	0.29	0.40	0.24	1	
Ni	0.71	0.86	0.59	0.72	0.71	0.71	1

The values represent coefficients of determination (R^2)

Table DR6. Chalcophile element contents (wt.%) of Kane Megamullion spinel harzburgites

			(ppm)								(ppb)		
Label	S	Cu	As	Zn	Ga	Pb	Se	Sb	Tl	Ni	Ag	Bi	Cd
5-1	159	40	35	68	1.6	0.5	2.6	1.5	0.24	1860	-	-	100
5-31A	142	17	3	56	11.7	0.6	0.5	-	0.06	1120	-	-	-
14-44	142	7	11	47	1.9	-	0.4	0.4	0.36	2050	-	-	-
14-70	81	9	5	43	3.9	-	0.3	-	0.13	1800	-	-	-
17-17	210	47	29	101	2.0	-	0.6	0.5	0.24	1590	-	-	-
19-10A	188	39	22	91	1.8	-	0.2	0.7	1.96	1810	-	20	100
19-11A	283	69	20	110	2.2	0.8	0.8	0.9	0.39	1720	-	-	-
19-18A	81	52	45	126	2.3	1.1	1.2	1.4	1.58	1870	-	70	-
19-31	215	59	45	111	2.4	0.7	-	2.1	1.71	1900	-	30	-
112-44A	241	11	5	72	1.2	0.7	1.6	0.3	0.14	1930	-	-	-
112-49	332	52	17	69	1.4	0.8	0.7	0.8	0.26	1670	-	20	-
112-71	84	21	23	82	2.1	0.9	-	1.4	0.28	1300	-	-	-
112-84	184	38	3	67	1.5	1.5	-	-	-	2030	-	-	-
113-40	129	14	25	50	1.2	0.6	0.1	0.3	0.63	1230	-	-	-
113-55A	561	21	22	127	3.0	1.0	-	1.8	3.30	1600	-	-	-
113-57A	32	25	10	115	1.8	0.8	-	0.4	0.41	1110	-	-	-
113-59A	45	23	9	171	1.6	0.9	-	0.4	0.70	1400	-	-	-
114-9	6	8	5	36	2.0	0.6	0.2	0.3	-	1380	-	20	-
114-19A	212	24	13	55	1.8	1.2	-	0.5	0.58	1610	90	100	-

The estimates of analytical precision (1 SD) are as follows: Cu, ±1.5%; Cd, ±33.3%; Ge, ±7.1%; Ga, ±1.5%; Pb, ±7.1%; Tl, ±1.5%; and were determined by repeated measurements of unknown samples. The estimates of analytical accuracy are as follows: As, ±3.7%; Cu, ±5.3%; Cd, ±14.6%; Ge, ±7.1%; Ga, ±17.0%; Hg, ±31.3%; Pb, ±4.5%; Sb, ±5.3%; Te, ±11.7%; Tl, ±10.6% and were determined by measurements of variuos certified material (GXR-1, GXR-4, GXR-6, SDC-1, SAR-M (U.S.G.S), DNC, SBC-1, DMMAS). After Ciazela et al. (under review, Geochimica et Cosmochimica Acta).

Table DR7. Major element contents (wt.%) of Kane Megamullion spinel harzburgites

Label	SiO_2	TiO_2	Al_2O_3	Fe_2O_3*	MnO	MgO	CaO	Na_2O	K_2O	P_2O_5	LOI	Total
5-1	38.6	0.02	1.21	9.07	0.13	36	1.25	0.07	0.01	0.04	12.9	99.2
5-31A	38.9	0.12	1.41	10.15	0.13	36.4	0.56	0.02	0.02	0.02	11.6	99.3
14-44	39.1	0.01	1.33	8.29	0.09	36.2	0.62	0.11	0.02	0.01	13.3	99.3
14-70	40.0	0.05	2.06	9.83	0.12	34.7	1.12	0.15	0.05	0.01	11.1	99.3
17-17	38.7	0.02	1.33	8.00	0.10	36.8	0.29	0.06	0.02	0.02	13.8	99.3
19-10A	34.8	0.02	1.06	8.54	0.17	32.5	5.87	0.08	0.02	0.03	16.1	99.3
19-11A	39.3	0.02	1.68	8.31	0.13	35.9	0.34	0.1	0.03	0.03	13.3	99.2
19-18A	37.6	0.04	1.58	11.31	0.16	33.5	1.81	0.14	0.03	0.07	12.9	99.2
19-31	36.5	0.02	1.71	9.38	0.15	31.6	5.28	0.15	0.01	0.07	14.1	99.1
112-44A	39.4	0.01	1.04	8.20	0.12	37.7	0.3	-	-	0.01	12.5	99.3
112-49	39.7	0.02	1.37	8.47	0.11	37.1	0.54	0.02	0.01	0.02	11.9	99.3
112-71	40.4	0.02	1.35	8.25	0.15	36	0.33	0.11	0.03	0.03	12.6	99.3
112-84	42.2	0.02	1.45	8.51	0.13	40.3	1.16	-	0.01	0.00	5.4	99.2
113-40	36.1	0.01	1.09	7.80	0.07	34.3	4.66	0.07	0.03	0.02	15.1	99.3
113-55A	40.4	0.12	1.78	15.09	0.20	33.8	1.79	0.16	0.02	0.09	5.8	99.3
113-57A	39.3	0.02	1.37	8.16	0.12	37.6	0.06	0.08	0.01	0.01	12.6	99.3
113-59A	38.5	0.01	1.07	10.52	0.14	36.9	0.03	0.05	0.01	0.01	12.2	99.4
114-19A	39.3	0.02	1.33	8.23	0.11	37.5	0.40	0.02	0.01	0.01	12.4	99.3

Fe_2O_3* = Total Fe as Fe_2O_3. LOI – loss-on-ignition. (-) below detection limit.

The estimates of analytical precision (1 SD) are between 1 and 2% and were determined by repeated measurements of unknown samples. After Ciazela et al. (under review, Geochimica et Cosmochimica Acta).